

Geodesic bifurcation on smooth surfaces

Hannes Thielhelm · Alexander Vais ·
Franz-Erich Wolter

© Springer-Verlag Berlin Heidelberg 2014

Abstract Within Riemannian geometry the geodesic exponential map is an essential tool for various distance-related investigations and computations. Several natural questions can be formulated in terms of its preimages, usually leading to quite challenging non-linear problems. In this context we recently proposed an approach for computing multiple geodesics connecting two arbitrary points on two-dimensional surfaces in situations where an ambiguity of these connecting geodesics is indicated by the presence of focal curves. The essence of the approach consists in exploiting the structure of the associated focal curve and using a suitable curve for a homotopy algorithm to collect the geodesic connections. In this follow-up discussion we extend those constructions to overcome a significant limitation inherent in the previous method, i.e. the necessity to construct homotopy curves artificially. We show that considering homotopy curves meeting a focal curve tangentially leads to a singularity that we investigate thoroughly. Solving this so-called geodesic bifurcation analytically and dealing with it numerically provides not only theoretical insights, but also allows geodesics to be used as homotopy curves. This yields a stable computational tool in the context of computing distances. This is applicable in common situations where there is a curvature induced non-injectivity of the exponential map. In particular we illustrate how applying geodesic bifurcation approaches the distance problem on compact manifolds with a single closed focal curve. Furthermore, the presented investigations provide natural initial values for computing cut loci using the medial differential equation which directly leads to a discus-

sion on avoiding redundant computations by combining the presented concepts to determine branching points.

Keywords Geodesic exponential map · Focal curves · Connecting geodesics · Distance computation · Cut locus · Voronoi diagram

1 Introduction

Distance-related problems including notions such as Voronoi diagrams or the cut locus are a central topic in computational geometry, where they are considered in Euclidean and also in more abstract settings, see e.g. [4]. Common discrete approaches dealing with non-Euclidean situations usually base or implicitly rely on a suitable approximation of the distance function $d_M(p, \cdot)$ with respect to some point p on the considered object M , see e.g. [14, 33]. The latter is commonly embedded into Euclidean space and discretized adequately. For example, combinatorial graph based techniques such as the Dijkstra algorithm typically perform a sweep over M emanating from p and extend every path which is distance minimizing. Even more sophisticated discrete distance approximations such as fast marching methods [10] basically iteratively extend a frontier of shortest paths and compare distances to preserve the minimizing property. As soon as a path ceases to be a globally shortest one, it is not considered anymore within such approaches as it loses its relevance for the discrete distance approximation.

The theory on Riemannian manifolds draws a much richer picture, incorporating curvature information to analyze the distance problem on M . Most notably it is well-known that shortest paths have the property of being locally straightest curves, known as geodesics, which are generalizations of the straight lines in the Euclidean setting. In the Riemannian case

H. Thielhelm (✉) · A. Vais · F.-E. Wolter
Welfenlab, Leibniz University of Hannover, Hannover, Germany
e-mail: thielhel@welfenlab.de

A. Vais
e-mail: vais@welfenlab.de

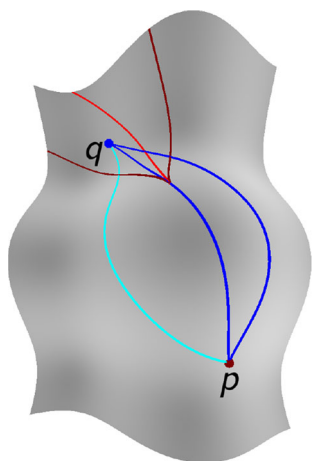


Fig. 1 Generic situation

not every geodesic has to be a shortest path. However, the reverse implication is true, therefore it is sufficient to search for shortest paths within the set of all geodesics connecting two given points $p, q \in M$. This is not possible within the commonly used discrete frameworks, since they lack the concept of a geodesic exponential map. Note that [25] introduces an exponential map in polyhedral settings paving the way to exploit the concept of geodesics within discrete settings.

The non-injectivity of the latter is captured in the cut locus. More precisely the cut locus of a point $p \in M$ is the closure of all points in M where a geodesic starting in p loses its distance minimizing property. Its relevance for the distance problem arises from the fact, that any geodesic not intersecting the cut locus is a shortest path. Consider Fig. 1 showing a surface patch and three geodesics connecting p and q . While the cyan geodesic is the shortest path, since it does not intersect the cut locus (light red), the blue geodesics lose their distance-minimizing property at their intersection points with the cut locus. We refer to such a set of connecting geodesics between p and q as distance relevant, since it contains the shortest path. Once such a set of geodesics is available determining the distance is essentially trivial as it amounts to choosing the shortest of them.

It is possible to obtain distance relevant sets of connecting geodesics without the use of the global cut locus concept relying on the local concept of focal curves. This approach has been pursued in [34], which we follow in this paper.

In Fig. 1 the focal curve of p , also known as the conjugate locus of p , is shown in dark red. Note that the cut locus begins in the so-called cusp of the focal curve. This situation is actually a generic representative of a curvature-induced cut locus branch, thereby focal cusps are considered to be natural starting points for tracing the cut locus.

Theoretical investigations for the cut locus can be found for example in [22, 28, 36, 37]. Computing cut loci and related concepts such as the medial axis or Voronoi diagrams based

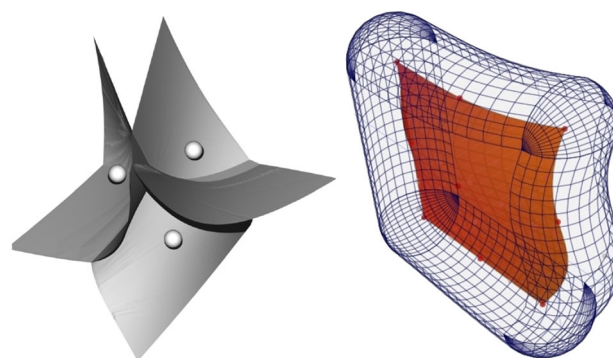


Fig. 2 Voronoi diagram and a medial axis. Proof of concepts in curved 3-space from [20, 21]

on discrete respectively smooth surface representations has received some attention in the literature, see e.g. [5, 6, 9, 16], respectively [30, 31]. The two and three-dimensional smooth Riemannian setting has been considered in [11, 19, 26] and [38, 39], the latter two being historical overviews on the respective computational methods. A proof of concept for the feasibility of computing three-dimensional Voronoi diagrams respectively medial axis inverse transformations in this case has been described in [20, 21], see Fig. 2 for exemplary results. However the corresponding two- and three-dimensional algorithms have been restricted to domains in which the exponential map is assumed to be injective, guaranteeing unique geodesic connections and thereby inducing situations that are topologically similar to the familiar Euclidean setting. For related theoretical investigations on how these restrictions can be expressed in terms of curvature dependent bounds see e.g. [13, 15, 23]. A survey on computational methods dealing with smooth surfaces can be found in [24]. In order to overcome the significant assumption of geodesic injectivity we recently started a more detailed investigation of the general two-dimensional Riemannian case [34]. We especially focus on a homotopy approach that generalizes to higher dimensions without exponentially increasing complexity. In order to illuminate the applicability of this approach within higher-dimensional distance related problems we present two-dimensional examples which should be understood as a proof of concept.

In this paper we extend upon the homotopy approach (HA) presented in [34] for computing multiple connecting geodesics on curved smooth surfaces. The HA collects a set of connecting geodesics between two arbitrary points p and q , making use of local concepts such as Jacobi fields and focal curves in a straight-forward manner as indicated by classical theory. Note that aside from distance computations connecting geodesics are of independent interest when considering them within a variational context as stationary points of a corresponding energy functional, see e.g. [1, 12].

The main subject of the HA is to exploit the generic situation shown in Fig. 1 where the Gaussian curvature of a surface patch causes a family of geodesics radiating from p to intersect among themselves. The resulting ambiguity of connecting geodesics is indicated by the presence of a focal curve. We refer to this situation as a locally caused non-injectivity of the geodesic exponential map. However, in general the ambiguity of connecting geodesics can also be caused by the topology of M , which we refer to as a global origin of non-injectivity. This is indicated by the existence of geodesic loops not generating focal points within M . A familiar example is the cylinder that exhibits geodesic loops even though it is intrinsically flat.

The HA is able to capture locally caused non-injectivities, indicating it to be a useful tool for distance computations on curved surfaces. However, a crucial part of the method is to construct a suitable homotopy curve, which has to intersect the focal curve transversally. In case the homotopy curve meets the focal curve tangentially the equations within the HA exhibit a singularity, the so-called geodesic bifurcation. This singularity excludes geodesics that generate a focal point as candidates for homotopy curves within the HA.

In this paper we fill this gap by studying and describing how to deal with the geodesic bifurcation. It turns out the examined singularity can be resolved enabling us to use geodesics as canonical homotopy curves within the HA. Since we base our approach on the ability to evaluate the geodesic exponential map, geodesics are a priori easily constructed homotopy curves in our context.

Additionally in a setting with closed focal curves our present contribution allows to compute the distance of arbitrary points without requiring the explicit knowledge of the cut locus or the focal curve. We exemplify how this solves the corresponding global distance problem on ellipsoidal shapes.

Our investigations of the geodesic bifurcation in focal cusps allow us to explain the singularity of the medial differential equation arising at the endpoints of the cut locus. Based on that we present a solution on how to deal with this singularity in practical applications. Within this discussion we explain the behaviour of medial curves in the presence of focal curves and furthermore combine the presented concepts to yield natural starting points for a redundancy minimizing approach to determine cut loci of discrete point sets, also commonly known as Voronoi diagrams.

Our approach is applicable to parametrized or implicit surfaces that allow the evaluation of second order derivatives, i.e. curvature information. This covers for example NURBS patches or subdivision surfaces [32], as well as manifold based constructions.

2 Basics

In this section we introduce some tools of Riemannian geometry, necessarily omitting some technicalities and details due to the lack of space. We follow the definitions and notations of [34] and recommend [3] for a detailed exposition to classical differential geometry that we build upon.

2.1 Riemannian manifolds

In this paper we assume M to be a two-dimensional complete Riemannian manifold with metric tensor $g = \langle \cdot, \cdot \rangle$. The latter is used to define the length of curves and induces a classical metric d_M on M . In many applications M is assumed to be a smooth surface embedded in Euclidean 3-space inheriting the ambient metric. However, our approach is designed to also cover the intrinsic setting which is naturally related to energy minimization problems as indicated by Maupertuis' principle, see [12].

The theorem of Hopf–Rinow assures the existence of shortest paths, which are curves realizing the distance between two arbitrary points $p, q \in M$. We denote the tangent space of M in p by T_pM and the vector resulting from a positive quarter turn of a tangent vector $v \in T_pM$ by v^\perp . Since the following considerations take place within a local context we do not distinguish between the objects on the manifold and their representation within a particular chart $x : U \subset M \rightarrow \mathbb{R}^2$. The latter map identifies points $p \in M$ with their coordinates $(x^1(p), x^2(p))$, simply denoted by (p^1, p^2) . In this paper assume $p \in M$ to be arbitrary, but fixed. Derivatives will be denoted as dotted quantities for functions of a single variable. We will often use the shorthand notation h_u for the partial derivative $\frac{\partial h}{\partial u}$.

In the next sections we will briefly discuss how to evaluate the geodesic exponential map, followed by a short review of concepts such as Jacobi fields, focal curves and the cut locus.

2.2 Geodesic polar coordinates (GPCs)

Geodesics on a Riemannian manifold can be understood as generalizations of the straight lines in Euclidean space. In order to investigate geodesics emanating from a given point p one usually introduces the geodesic exponential map, denoted by $\exp_p : T_pM \rightarrow M$, mapping $s \cdot v(\varphi) \in T_pM$ to the endpoint of the geodesic γ_φ starting in p in the direction $v(\varphi) \in S^1 \subset T_pM$ with length s . The computation of the geodesic $\gamma = \gamma_\varphi : [0, s] \rightarrow M$ is realized by solving the geodesic differential equations $\nabla_{\dot{\gamma}} \dot{\gamma} = 0$, where ∇ is the Levi–Civita connection on M . To evaluate \exp_p in practice one has to compute the coordinates of γ . This amounts to solving

$$\ddot{\gamma}^k + \Gamma_{ij}^k \dot{\gamma}^i \dot{\gamma}^j = 0$$

starting in a chart covering p with the initial values $\gamma^l(0) = p^l, \dot{\gamma}^l(0) = v^l$ and performing chart transitions during the integration if necessary. The Γ_{ij}^k are the Christoffel symbols of ∇ and given by

$$\Gamma_{ij}^k = \frac{1}{2}g^{mk} \left(\frac{\partial g_{im}}{\partial x^j} + \frac{\partial g_{jm}}{\partial x^i} - \frac{\partial g_{ij}}{\partial x^m} \right),$$

where (g_{ij}) is the representation of the metric tensor g with respect to the frame induced by the current chart and (g^{jk}) denotes its inverse.

Since the geodesics we use are by definition arc-length parametrized, the parameters (s, φ) introduced by the map $O_p : (s, \varphi) \mapsto \gamma_\varphi(s)$ are said to be geodesic polar coordinates (GPCs) with respect to p on M . Note that O_p is not injective in general for $s \geq r_p$, where r_p is chosen minimally and said to be the injectivity radius of M with respect to p . In case r_p is finite O_p does not equip M with proper coordinates in a unique manner. The theorem of Hopf–Rinow however states that O_p is surjective, so that for any point q in M there exists at least some s_0, φ_0 with $O_p(s_0, \varphi_0) = q$. The corresponding geodesic γ_{φ_0} is called a connecting geodesic of $p = \gamma(0)$ and $q = \gamma(s_0)$.

The GPC concept allows us to define a geodesic circle with center $p \in M$ and radius $s > 0$ as being the set of all points $\{O_p(s, \varphi) : \varphi \in S^1\}$ which is a superset of the distance circle $\{q \in M : d_M(p, q) = s\}$.

We will now discuss the injectivity of O_p incorporating the classical concepts of focal curves respectively the cut locus.

2.3 Focal curves

To investigate the local injectivity of O_p in terms of focal curves we have to consider the vector field $J_{\varphi_0}(s) = \frac{\partial}{\partial \varphi} O_p(s, \varphi_0)$ along the geodesic $\gamma = \gamma_{\varphi_0}$ for a fixed φ_0 . From the Lemma of Gauss it is evident, that $J_{\varphi_0}(s) \perp \dot{\gamma}_{\varphi_0}(s)$ and therefore $J_{\varphi_0}(s) = y(s, \varphi_0)\dot{\gamma}_{\varphi_0}^\perp(s)$ respectively

$$\frac{\partial}{\partial \varphi} O_p(s, \varphi_0) = y(s, \varphi_0) \frac{\partial}{\partial s} O_p(s, \varphi_0)^\perp \tag{1}$$

with a scalar function $y(\cdot) = y(\cdot, \varphi_0)$. It is a well-known result that y satisfies the scalar Jacobi equation

$$\ddot{y}(s) + K(\gamma(s))y(s) = 0,$$

where $K(\gamma(s))$ is the Gaussian curvature of M in $\gamma(s)$. In practice the computation of y is realized by solving the above differential equation simultaneously to the geodesic differential equation for γ . Initial values for the considered Jacobi field are given by $y(0) = 0$ respectively $\dot{y}(0) = 1$. See [34] for a derivation of the scalar Jacobi equation from its classical formulation. Roughly spoken the spreading of infinitesimally nearby geodesics in our two-dimensional setting is encoded into y and is closely related to Gaussian curvature as described by the Jacobi equation.

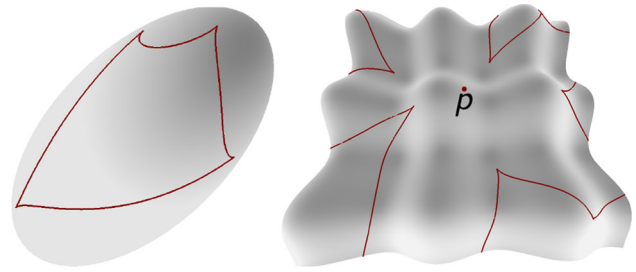


Fig. 3 Closed respectively unbounded focal curves

A point $a = O_p(s_0, \varphi_0)$ is said to be conjugate to p if $y(s_0, \varphi_0) = 0$. In general geodesics can generate multiple focal points while they extend, but since we use focal points as an indicator for non-injectivity we will direct our attention to the first ones. The set of all these points is called the (first) conjugate locus. A generalization of the conjugate locus of p incorporating the Fermi coordinates with respect to a curve c on M instead of GPCs leads to the notion of focal curves [3]. Since the HA generalizes to yield connecting geodesics emanating orthogonally from c , we will use the name focal curve instead of conjugate locus. Thus, we say that the geodesic γ_{φ_0} generates the focal point a , and denote by f_p the set of all focal points with respect to p .

If $O_p(s_0, \varphi_0)$ is a focal point then O_p is not injective in any neighborhood of (s_0, φ_0) since the differential

$$DO_p = \begin{pmatrix} \frac{\partial O_p}{\partial s} & \frac{\partial O_p}{\partial \varphi} \end{pmatrix} = \begin{pmatrix} \dot{\gamma}_{\varphi_0} & y\dot{\gamma}_{\varphi_0}^\perp \end{pmatrix}$$

is singular as $y(s_0, \varphi_0)$ vanishes [29]. In fact f_p can be understood as bordering a region of local non-injectivity of the exponential map.

The success of finding all relevant geodesic connections from p within the HA depends on the specific choice of the homotopy curve and its interaction with f_p . In order to construct suitable homotopy curves it is useful to distinguish two different types of focal curves.

The focal radius $s_f : S^1 \rightarrow \mathbb{R} \cup \{\infty\}$ is implicitly defined by $y(s_f(\varphi), \varphi) = 0$, where $s_f(\varphi)$ is chosen to be minimal (thereby capturing the distance to the first occurrence of a focal point) or set to ∞ if γ_φ does not generate a focal point. Let $D \subseteq S^1$ be the set, where s_f is finite. A focal curve is said to be closed if $D = S^1$, as for example on the ellipsoid in Fig. 3. Otherwise, D consists of disjoint intervals of S^1 and we say that every connected component of f_p corresponding to such an interval is unbounded. We will by abuse of language also refer to one component of f_p as a focal curve of p . See Fig. 3 on the right for a couple of unbounded focal curves on a height surface.

Consider now a focal curve of p , parametrized by $f_p(\varphi) = O_p(s_f(\varphi), \varphi)$. Differentiating yields

$$\dot{f}_p(\varphi) = \dot{s}_f(\varphi) \frac{\partial O_p}{\partial s}(s_f(\varphi), \varphi) = \dot{s}_f(\varphi) \dot{\gamma}_\varphi(s_f(\varphi)), \quad (2)$$

where γ_φ generates the focal point $f_p(\varphi)$. We say that $f_p(\varphi)$ is a regular focal point if $\dot{f}_p(\varphi) \neq 0$ and conclude from the last equation that the geodesic γ_φ generating the focal point $f_p(\varphi)$ meets f_p tangentially at that point. Since \dot{f}_p vanishes at points where s_f becomes extremal we refer to such focal points as focal cusps. Differentiating $y(s_f(\varphi), \varphi) = 0$ one obtains

$$\dot{s}_f(\varphi) = -\frac{y_\varphi(s_f(\varphi), \varphi)}{y_s(s_f(\varphi), \varphi)},$$

where the denominator never vanishes as discussed in [34]. A focal cusp $O_p(s_0, \varphi_0)$ is therefore characterized by $y_\varphi(s_0, \varphi_0) = 0$ in addition to $y(s_0, \varphi_0) = 0$.

2.4 Cut locus

Regarding the global injectivity of O_p one usually considers the concept of the cut locus [3,36]. An important difference between the cut locus C_p and the focal curve f_p of a point $p \in M$ is that the latter is defined in terms of locally available information, i.e. it requires only knowledge of the metric tensor along the geodesic generating the considered focal point. The cut locus however is defined in a global sense, since it incorporates the global notion of a shortest path.

Let $s_c(\varphi) \in \mathbb{R} \cup \{\infty\}$ denote the minimal parameter value such that the geodesic $s \mapsto \gamma_{\varphi_0}(s)$ stops being a shortest path for $s > s_c(\varphi)$. It is useful to set $s_c(\varphi) = \infty$, if the geodesic γ_φ remains a shortest path while it extends infinitely. Then the cut locus of p is given by

$$C_p = cl \left\{ O_p(s_c(\varphi), \varphi) \mid \varphi \in S^1, s_c(\varphi) < \infty \right\},$$

where cl denotes the topological closure. It is well-known that $r_p \leq s_c(\varphi) \leq s_f(\varphi)$, i.e. the exponential map loses its global injectivity in general before this becomes locally noticeable.

A focal point $f_p(\varphi)$ where $s_f(\varphi) = s_c(\varphi)$ has to be a focal cusp that is locally accessible as indicated by $y_\varphi(s_f(\varphi), \varphi) = 0$. Furthermore it lies on the topological boundary of C_p .

In order to generalize our discussion, it is appropriate to consider a finite discrete set of reference points $P = \{p_1, \dots, p_n\}$ instead of just a single point p . In order to distinguish between the reference points and other points on M it will be convenient to also refer to the elements of P as sites. We define the cut locus C_P of P as the closure of the set of all points having at least two shortest paths to elements of P . This definition is compatible with the above cut locus definition for a single reference point, [35]. Furthermore it generalizes the typical notion of the

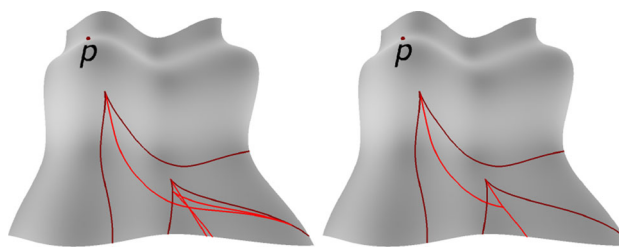


Fig. 4 Symmetry set and cut locus

Voronoi diagram V_P of P , the latter being usually defined in terms of a distance partition of M into Voronoi regions $R(p) = \{q \in M : d(p, q) \leq d(r, q) \forall r \in P\}$, whose boundaries $\cup_{p \in P} \partial R(p)$ form V_P . It can be shown that in general $V_P \subset C_P$, whereas in the Euclidean setting both notions coincide. Note that while the cut locus concept is even more general as it allows for an arbitrary closed subset of M to be used as a reference set, we will focus in this paper on the definition given above, conveniently denoting C_P also as the (geodesic) Voronoi diagram of P .

Its local counterpart is called the symmetry set S_P of $P = \{p_1, \dots, p_n\}$ as given by

$$S_P = cl \left\{ m \mid m = O_{p_i}(s, \varphi) = O_{p_j}(s, \psi), (i, \varphi) \neq (j, \psi) \right\}$$

i.e. as the closure of all points $m \in M$, which are connected with two distinct points $p_i, p_j \in P$ via (at least) two geodesics of equal length. The cut locus C_P is contained in the symmetry set S_P , see e.g. Fig. 4, which by construction can be determined using the medial equation

$$O_p(s(\lambda), \varphi(\lambda)) = O_q(s(\lambda), \psi(\lambda)). \quad (3)$$

By differentiating this equation with respect to λ one obtains the so-called medial differential equation (MDE, [27]), which will be used later on to determine geodesic Voronoi diagrams.

2.5 Structure of geodesic Voronoi diagrams

In the following we discuss the structure of geodesic Voronoi diagrams on a smooth surface which in the two-dimensional case is known to be a graph, c.f. [17,18], consisting of multiple branches. In contrast to the cut locus consisting of branches we say that the symmetry set consists of medials, the latter being described by the medial equation. As explained above each branch of the cut locus is contained in the corresponding medial. We therefore first discuss the structure of the medials and afterwards focus on the branching behaviour of the cut locus, characterizing the latter in terms of circumcircles.

For our purposes it is convenient to distinguish between locally and globally induced medials with the corresponding cut locus branches being named analogously. More precisely we will call a medial beginning respectively ending in

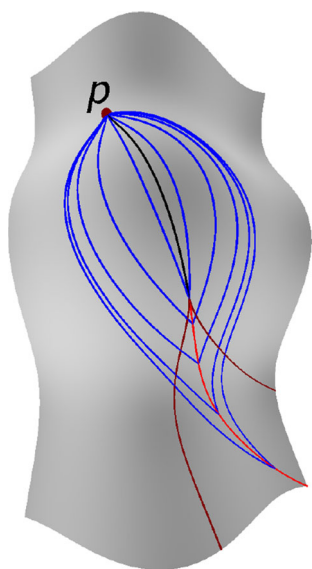


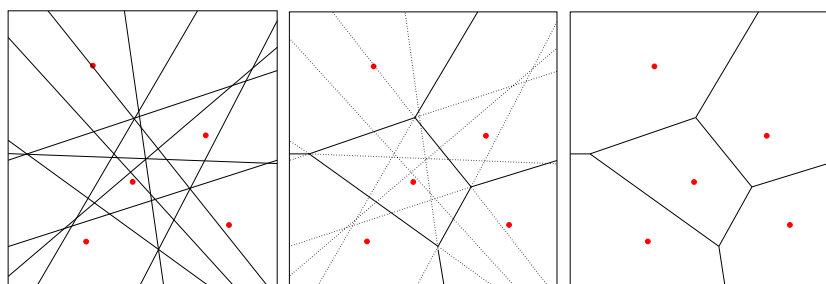
Fig. 5 Two families of geodesics tracing a cut locus branch.

a focal cusp locally induced, whereas it is said to be globally induced otherwise. According to this definition any medial arising from considering the medial equation with two distinct reference points is globally induced.

As an example for a locally induced medial consider Fig. 5. The light red medial is traced by two families of geodesics (blue) starting in p as described by the medial differential equation [with $q = p$ in Eq. (3)]. Those families degenerate to a single geodesic (black) connecting p and the focal cusp, where the MDE becomes singular. However, the endpoint of the black geodesic is a point on the medial, which is locally accessible, as it is characterized as a focal cusp. The splitting of the single black geodesics into a pair of blue geodesics is closely related to the geodesic bifurcation of the geodesic generating the focal cusp, see Sect. 3.3, and discussed in the context of natural starting points in Sect. 4.3.

Examples for globally induced medials are bisectors within a Voronoi diagram or the cut locus of a single reference point on an unbounded cylinder. Notice that in both cases one obtains a point on the medial as soon as one knows a distance minimizing connecting geodesic [34] by using the middle point on the corresponding geodesic.

Fig. 6 Redundant segments of medials



Having briefly discussed medials we will now outline how the intersections of medials give rise to the branching points of the cut locus. For this consider the Voronoi diagram for the five sites (colored red) shown in Fig. 6 on the right. It is trivially contained in the respective symmetry set shown on the left, which consists of several medials. In case the metric of the ambient surface is not Euclidean each of those medials is traced via the MDE incorporating appropriate initial points, as discussed later in Sect. 4.3. However, proceeding in this way one has to compute an initial point and a medial for each pair of sites, resulting in redundant computations. This redundancy becomes evident in our example, where five sites induce ten different medials (left) of which the dotted segments (middle) are unnecessary, producing the final result (right).

In order to characterize the branching points of a geodesic Voronoi diagram C_P , note that every branching point b in C_P has at least three distinct shortest geodesic connections to the sites in P , thereby determining a distance circle containing no sites in its interior. We will call such a circle circumcircle of the respective sites and its center b circumcenter. Our five site example contains four such relevant circumcircles, with one of those being depicted on the right of Fig. 6.

Note that contrary to the Euclidean case the considered connecting geodesics of a circumcircle can end up on the same site. Furthermore, the circumcenters respectively circumcircles do not need to be uniquely determined by three given sites. In fact the presented Riemannian generalizations of the familiar Euclidean concepts exhibit many non-trivial phenomena, which we encounter in applications as witnessed in Sect. 4. This necessitates the tools developed and presented in the following sections.

2.6 Derivatives

In this paper we will frequently deal with medials and homotopy curves, being curves on M described by GPCs via $\lambda \mapsto O_p(s(\lambda), \varphi(\lambda))$. The tangent of such a curve is directly given within the frame $\frac{\partial O_p}{\partial s}, \frac{\partial O_p}{\partial s}^\perp$. The vector $\frac{\partial O_p}{\partial s}$ is directly obtained from the geodesic differential equation and $\frac{\partial O_p}{\partial \varphi} = y \frac{\partial O_p}{\partial s}^\perp$ is calculated by solving the Jacobi equation for y .

The higher order derivatives of O_p can be expressed via the partial derivatives of y , which is calculated by solving the differentiated Jacobi equation discussed in [34]. First of all $\frac{\nabla}{\partial s} \frac{\partial O_p}{\partial s} = \nabla_{\dot{\gamma}} \dot{\gamma} = 0$ by the definition of a geodesic, implying $\frac{\nabla}{\partial s} \frac{\partial O_p}{\partial s}^\perp = 0$. Since $\frac{\partial O_p}{\partial s}$ and $\frac{\partial O_p}{\partial \varphi}$ are the basis fields induced by geodesic polar coordinates, their Lie bracket vanishes. Taking into account that the Levi-Civita connection ∇ is torsion-free [3], this yields

$$\frac{\nabla}{\partial \varphi} \frac{\partial O_p}{\partial s} = \frac{\nabla}{\partial s} \frac{\partial O_p}{\partial \varphi},$$

For the derivatives with respect to the family parameter λ we obtain the useful expressions

$$\begin{aligned} \frac{\nabla}{d\lambda} \frac{\partial O_p}{\partial s} &= \frac{\nabla}{\partial s} \frac{\partial O_p}{\partial s} \dot{s} + \frac{\nabla}{\partial \varphi} \frac{\partial O_p}{\partial s} \dot{\varphi} = \frac{\nabla}{\partial s} \frac{\partial O_q}{\partial \varphi} \dot{\varphi} \\ &= \frac{\nabla}{\partial s} \left(y \frac{\partial O_p}{\partial s}^\perp \right) \dot{\varphi} = y_s \dot{\varphi} \frac{\partial O_p}{\partial s}^\perp, \end{aligned}$$

$$\frac{\nabla}{d\lambda} \frac{\partial O_p}{\partial s}^\perp = -y_s \dot{\varphi} \frac{\partial O_p}{\partial s}.$$

3 Contribution

In this section we extend the homotopy approach for computing connecting geodesics described in [34]. We begin by recalling this method briefly and motivate the geodesic bifurcation, which is investigated and discussed afterwards. Building on these results we describe how to use the geodesic bifurcation within the homotopy approach.

In general, surfaces can have a complicated distribution of positive and negative Gaussian curvature. To illustrate our approach we have included several pictures based on numerical examples calculated using an implementation of the presented methods, focusing on the surface parametrized by $f(u, v) = (u, v, \cos(u) + \sin(v))$, if not stated otherwise. While our methods deal with arbitrarily parametrized surfaces, possibly compact and covered with many charts, we have chosen this didactic example with regard to its rich presence of focal curves and the abundantly occurring associated phenomena studied in this paper. Please also note that the appearing boundaries are in fact a necessity of the visualization as all considered manifolds have no boundary.

3.1 Homotopy approach (HA)

For a brief illustration of the method we focus on the generic situation shown in Fig. 7, where the curvature of a surface patch causes the geodesics emanating from p to intersect, as indicated by the presence of a focal curve f_p , colored in dark red. We have placed a point q within the region bordered by

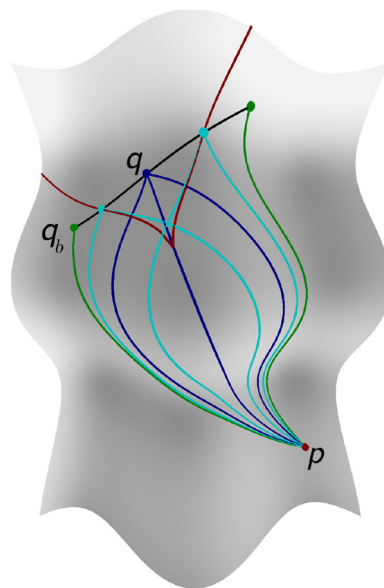


Fig. 7 Generic situation for the HA

the focal curve, which we will call the focal region within this example.

In order to calculate the connecting geodesics between p and q , [34] suggests to construct a regular curve $Q : I \rightarrow M$ (black) passing through q . This so-called homotopy curve Q can be chosen arbitrarily to a large extent, except that it has to intersect the focal curve transversally and should start and end outside the focal region. Furthermore the homotopy curve is constructed to yield a geodesic connecting p with its start point $O_p(s_b, \varphi_b) = Q(t_b) = q_b$. A homotopy curve satisfying all these properties will be called valid (within the HA). The HA allows for tracing a component of the one-dimensional solution set S of $O_p(s, \varphi) = Q(t)$, yielding a solution curve $S : \lambda \mapsto (s(\lambda), \varphi(\lambda), t(\lambda))$.

The solution set S contains information about the connecting geodesics between every point on the curve Q and p in this setting. More precisely, if $q = Q(t_q)$, the initial values of the corresponding connecting geodesics are given by the GPCs of q :

$$\{(s_q, \varphi_q) \mid (s_q, \varphi_q, t_q) \in S\}.$$

We refer to the process described above of determining the solution curve $S(\lambda)$ within the HA by saying that *the curve Q is traced by the family of geodesics $\gamma_{\varphi(\lambda)} = O_p(\cdot, \varphi(\lambda))$.*

Figure 8 depicts the projection of the solution curve into the (t, φ) parameter plane and illustrates how to collect the three (blue) geodesic connections from p to q by considering that $q = Q(t_q)$. Within our prototypical setting and exemplified by Fig. 8, it is obvious that every point lying on Q and contained in the interior of the focal region has exactly three connecting geodesics (blue) to p , while those points on the border have two (cyan). The connecting geodesics from the

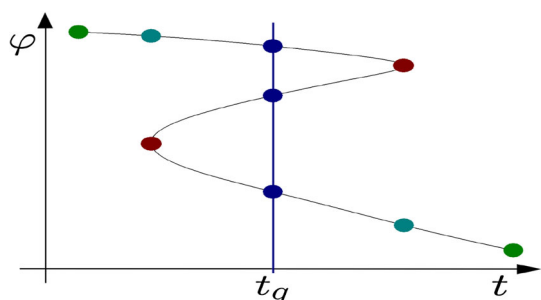


Fig. 8 Solution curve of the HA in (t, φ) -space

points on Q , which are outside the focal region are unique (green). The characteristic behavior of the (t, φ) -solution in its extremal points is phrased by saying that *the family $\gamma_{\varphi(\lambda)}$ is reflected* by the focal curve, i.e. it reflects at points where the corresponding geodesic generates a focal point, marked dark red. For a more detailed explanation of the HA see [34].

3.2 Geodesic bifurcation

In order to explain and understand the geodesic bifurcation we have to examine the solution curves obtained by tracing a collection of homotopy curves. For this purpose consider the left part of Fig. 9 depicting three different homotopy curves starting in q_b . The right part shows projections of the corresponding solution curves in the (s, φ) parameter plane. It also visualizes the focal curve f_p via $s_f(\varphi)$ in dark red appearing as a kind of parabola opening in s -direction with its lower part corresponding to the left arc of f_p . The blue curve on the left is a valid homotopy curve as it starts and ends outside of the focal region bordered by f_p while crossing f_p transversally and the same applies for the green curve, although it is closer to being tangential to the left arc of the focal curve. The cyan curve misses the left arc of the focal curve completely and does not end outside the focal region, i.e. it is not valid.

The corresponding solution curves in the parameter diagram for the valid homotopy curves consist of one connected component. However, the cyan solution set consists of two connected components. The HA would only trace the upper

component of it, while the lower remains locally inaccessible.

Imagine the three cases shown to be embedded within a one-parameter family of homotopy curves and corresponding configurations in the (s, φ) -plane. In this family we can expect one homotopy curve to meet the focal curve tangentially. Note that the HA as presented in [34] fails for such homotopy curves, i.e. excluding geodesics generating a focal point from being used as homotopy curves. In the following we will explicitly deal with this tangential situation.

The solution curve $S : \lambda \mapsto (s(\lambda), \varphi(\lambda), t(\lambda))$ within the HA is characterized by

$$O_p(s(\lambda), \varphi(\lambda)) = Q(t(\lambda)). \tag{4}$$

Differentiating with respect to λ and using (1) yields

$$\dot{s} \frac{\partial O_p}{\partial s} + y \dot{\varphi} \frac{\partial O_p^\perp}{\partial s} = i \dot{Q}, \tag{5}$$

In order to determine the tangent vector $\dot{S}(\lambda)$, consider taking scalar products to obtain

$$\dot{s} = \left\langle \dot{Q}, \frac{\partial O_p}{\partial s} \right\rangle i \quad y \dot{\varphi} = \left\langle \dot{Q}, \frac{\partial O_p^\perp}{\partial s} \right\rangle i. \tag{6}$$

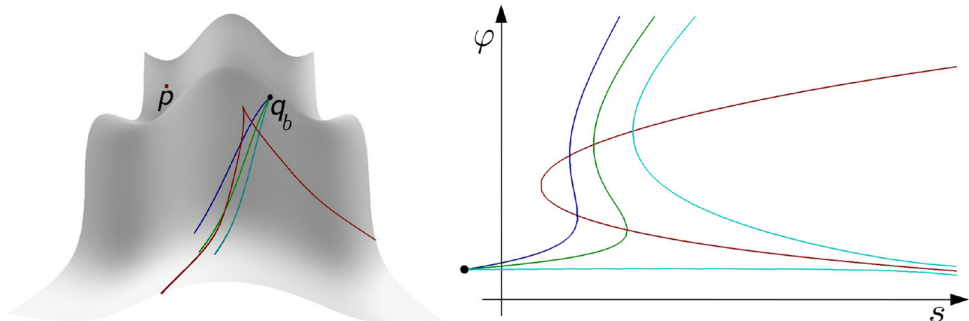
Without loss of generality we assume Q to be parametrized by arc length. Then the above equations, together with the additional condition $\dot{s}^2 + \dot{\varphi}^2 + \dot{t}^2 = 1$, can be solved for $\dot{S}(\lambda) = (\dot{s}, \dot{\varphi}, \dot{t})$ uniquely up to orientation, provided that y and $\left\langle \dot{Q}, \frac{\partial O_p^\perp}{\partial s} \right\rangle$ do not vanish simultaneously. This tangent information can be used within classical numerical ODE solvers or predictor-corrector methods as discussed in [34].

Consider now a point $S(\lambda_0) = (s_0, \varphi_0, t_0)$ on the solution curve, where the above equations become singular and cannot be uniquely solved, i.e. we have

$$y(s_0, \varphi_0) = 0 \Leftrightarrow Q(t_0) \in f_p, \\ \left\langle \dot{Q}(t_0), \frac{\partial O_p}{\partial s}(s_0, \varphi_0)^\perp \right\rangle = 0 \Leftrightarrow \dot{Q}(t_0) \parallel \dot{\gamma}_{\varphi_0}.$$

Using Eq. (2) we conclude that Q has to meet the focal curve f_p tangentially in $Q(t_0)$ in order for the Eq. (6) to become singular and vice versa. In this case, we still obtain $\dot{s}_0 = \dot{t}_0$,

Fig. 9 Two valid curves (green, blue) and one non-valid homotopy curve (cyan) and their preimages under O_p



but cannot infer $\dot{\varphi}_0$ from (6) indicating that the solution set of (4) does not necessarily have the topology of a curve. In fact, it will turn out that it consists of two branches meeting in (s_0, φ_0, t_0) .

In the following we use the shorthand notation $\dot{s}_0 = \dot{s}(\lambda_0)$, $\dot{\varphi}_0 = \dot{\varphi}(\lambda_0)$, etc. The tangential vectors $(\dot{s}_0, \dot{\varphi}_0)$ of those branches in the intersection point (s_0, φ_0) cannot be obtained from the first-order derivatives. Instead one may apply L'Hôpital or equivalently differentiate Eq. (5) again with respect to λ yielding

$$\begin{aligned} \ddot{s} \frac{\partial O_p}{\partial s} + \dot{s} \frac{\nabla}{\partial \lambda} \frac{\partial O_p}{\partial s} + (y_s \dot{\varphi} + y \ddot{\varphi}) \frac{\partial O_p^\perp}{\partial s} + y \dot{\varphi} \frac{\nabla}{\partial \lambda} \frac{\partial O_p^\perp}{\partial s} \\ = i \frac{\nabla}{\partial \lambda} \dot{Q} + \ddot{i} \dot{Q}, \end{aligned}$$

where the partial derivatives of O_p respectively y are evaluated in (s_0, φ_0) . Using the derivatives introduced in Sect. 2.6 and collecting terms, one obtains

$$\begin{aligned} (\ddot{s} - y y_s \dot{\varphi}^2) \frac{\partial O_p}{\partial s} + (y \ddot{\varphi} + 2y_s \dot{s} \dot{\varphi} + y_\varphi \dot{\varphi}^2) \frac{\partial O_p^\perp}{\partial s} \\ = i \frac{\nabla}{\partial \lambda} \dot{Q} + \ddot{i} \dot{Q}. \end{aligned} \tag{7}$$

Substituting $y(s_0, \varphi_0) = 0$ and using the geodesic curvature κ of Q to express

$$\frac{\nabla}{\partial \lambda} \dot{Q}(t_0) = \kappa(t_0) \dot{Q}^\perp(t_0) = \kappa(t_0) \frac{\partial O_p^\perp}{\partial s}(s_0, \varphi_0),$$

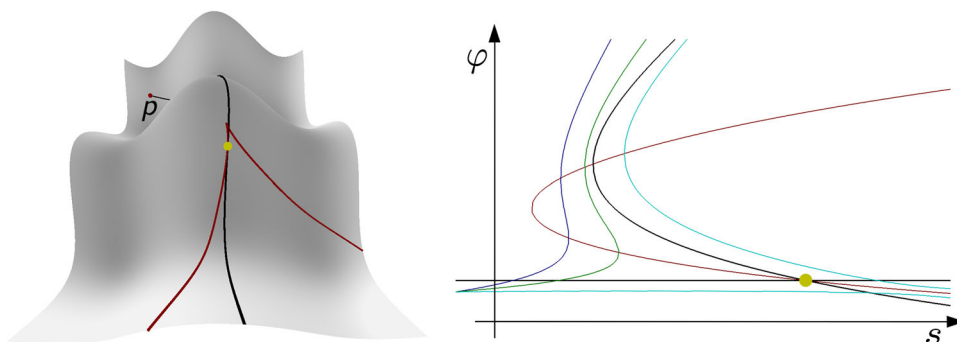
equation (7) simplifies to

$$\begin{aligned} \ddot{s}_0 \frac{\partial O_p}{\partial s} + (y_\varphi \dot{\varphi}_0^2 + 2y_s \dot{s}_0 \dot{\varphi}_0) \frac{\partial O_p^\perp}{\partial s} \\ = \ddot{i}_0 \frac{\partial O_p}{\partial s} + \dot{i}_0 \kappa(t_0) \frac{\partial O_p^\perp}{\partial s}. \end{aligned}$$

By comparing coefficients we obtain $\ddot{s}_0 = \ddot{i}_0$ and a quadratic equation for $\dot{\varphi}_0$:

$$y_\varphi \dot{\varphi}_0^2 + 2y_s \dot{s}_0 \dot{\varphi}_0 - \dot{i}_0 \kappa(t_0) = 0.$$

Fig. 10 Geodesic (black) as homotopy curve and its solution branches within the HA in black



At this point, the presence of the two possible values

$$\dot{\varphi}_0 = \frac{-y_s \dot{s}_0 \pm \sqrt{y_s^2 \dot{s}_0^2 + \dot{i}_0 \kappa(t_0) y_\varphi}}{y_\varphi} \tag{8}$$

analytically illuminates the existence of two solution branches meeting in (s_0, φ_0, t_0) . Therefore, we speak of a geodesic bifurcation occurring.

The projection of the solution set S into the (s, φ) -plane is colored in black in the example shown in Fig. 12 and consists of two differentiable solution branches meeting in the bifurcation point (s_0, φ_0) . These become accessible using the tangent information from Eq. (8) together with $\dot{s}_0 = \dot{i}_0$ from Eq. (6).

Using this tangent information adequately within the HA, as described in Sect. 3.4, the method yields two families of geodesics tracing Q , which correspond to the two solution branches. Therefore we consider curves, which meet the focal curve tangentially, and especially geodesics generating focal points from now on as valid homotopy curves.

3.3 Geodesics as homotopy curves

From now on consider the homotopy curve Q to be a geodesic γ_{φ_0} , which generates the focal point $O_p(s_0, \varphi_0)$. As Q is a geodesic, we have $\kappa(t_0) = 0$ in Eq. (8). In this case the tangent directions of the two solution branches in the bifurcation point are given by

$$\dot{s}_0 = \dot{i}_0 \quad \text{and} \quad \left(\dot{\varphi}_0 = 0 \quad \text{or} \quad \dot{\varphi}_0 = -2\dot{i}_0 \frac{y_s}{y_\varphi} \right). \tag{9}$$

These branches are illustrated in Fig. 10, fitting into the collection of solution sets depicted in Fig. 9. The black straight line $\varphi = \varphi_0$ in the parameter diagram corresponds trivially to the (black) geodesic γ_{φ_0} . The curved branch colored in black in the parameter diagram is the one we are interested in. It becomes accessible using the non-trivial tangent information from the last equation.

Since the equations for the tangent information in the bifurcation/focal point require $y_\varphi(s_0, \varphi_0)$ not to vanish, they cannot be used when $O_p(s_0, \varphi_0)$ is a focal cusp. We consider

now this remaining case. The derived equations are not sufficient to obtain the tangent information in this very special case, which requires differentiating Eq. (7). Despite the compact presentation using the notational shortcuts outlined in Sect. 2.6, it turns out that these calculations are quite tedious, though straightforward. Performing them yields besides $\dot{s}_0 = 0$:

$$\ddot{s}_0 = \ddot{t}_0, \quad \dot{\varphi}_0 = 0 \quad \text{or} \quad \dot{\varphi}_0 = \pm \sqrt{-3\ddot{t}_0 \frac{y_s}{y_{\varphi\varphi}}}. \quad (10)$$

In addition the same calculations can be used to determine the higher order derivative $\ddot{\varphi}_0$ in every regular bifurcation point: Here we already have $\ddot{s}_0 = \ddot{t}_0$ and obtain

$$\ddot{\varphi}_0 = 4y_{s\varphi} \frac{y_s}{y_{\varphi}^2} - \frac{8}{3} y_{\varphi\varphi} \frac{y_s^2}{y_{\varphi}^3}. \quad (11)$$

Note that the presented equations in this section for the tangent or higher order information are only valid in the bifurcation point (s_0, φ_0, t_0) . However, they can obviously be used to obtain first respectively second order Taylor approximations of the solution branches, as shown in green respectively blue in Fig. 13 on the left. We have used a second respectively first order Taylor approximation for s respectively φ in the focal cusp to yield the green parabola approximating the black solution branch in the figure on the right.

3.4 Geodesic bifurcation within the HA

Up to now we were mainly interested in the bifurcation phenomenon to resolve the singularity of the exponential map in a focal point. In the following we combine the equations for the tangent information in non-singular points (6) and in the bifurcation points (9) in order to use geodesics, which generate a focal point, as homotopy curves within the HA.

Again, the homotopy curve Q is a geodesic γ_{φ_0} generating a focal point at $O_p(s_0, \varphi_0)$. The point (s_0, φ_0, t_0) with $t_0 = s_0$ is the bifurcation point in the parameter space, i.e. it lies on the non-trivial solution branch and serves as an initial value to start tracing it. At this point, one has to use the tangent information from Eq. (9) to perform an initial step away from the singular bifurcation point and the trivial solution branch

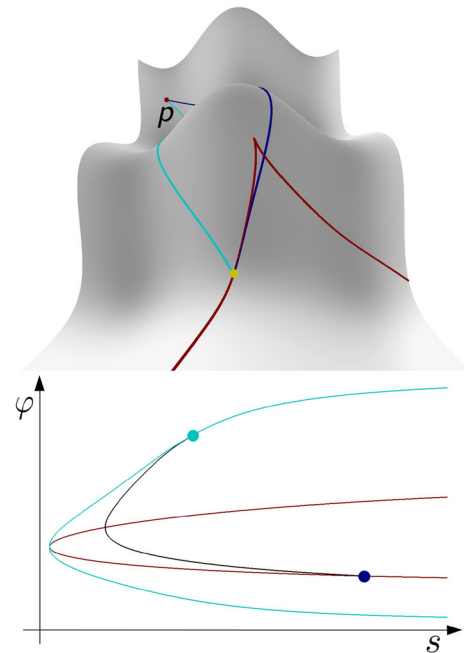


Fig. 12 Two solution branches meeting in (s_0, φ_0)

$\varphi = \varphi_0$. This can be achieved using a small Euler integration step based on the first order Taylor approximation using a small step $\dot{t} = \Delta\lambda$:

$$\varphi_1 = \varphi_0 - 2 \frac{y_s}{y_{\varphi}} \Delta\lambda, \quad s_1 = s_0 + \Delta\lambda, \quad t_1 = t_0 + \Delta\lambda$$

The sign of $\dot{t} = \Delta\lambda$ actually determines the tracing direction on the solution path. A more accurate initial step is obtained by using the second order information given by Eq. (11). Now the point (s_1, φ_1, t_1) serves as an initial value suitable for obtaining a family of geodesics tracing Q as described by Eq. (6).

From now on we will refer to performing the HA with a geodesic γ_{φ_0} (which generates a focal point) as homotopy curve, simply as *applying geodesic bifurcation to the geodesic γ_{φ_0}* . This process is illustrated in Fig. 11 where the geodesic γ_{φ_0} is colored black. The green geodesics are obtained by tracing γ_{φ_0} upwards. The purple geodesics trace it down-

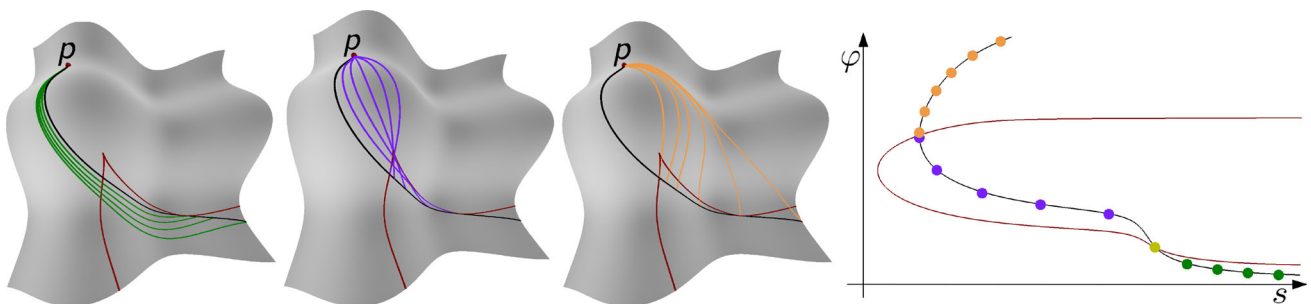
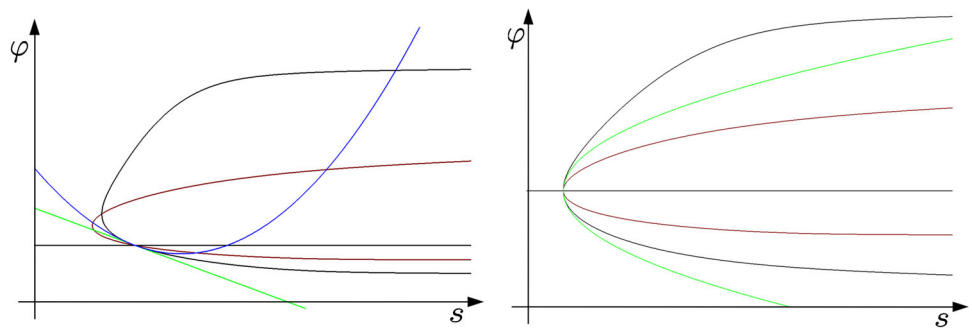


Fig. 11 Family of geodesics tracing the black geodesic obtained by applying geodesic bifurcation

Fig. 13 *Left* First (green) and second (blue) order Taylor approximation of the solution branch (black) in a regular focal point. *Right* Mixed Taylor approximation (green) of the solution branch (black) in a focal cusp



wards, whereas after reflection tracing continues upwards along γ_{φ_0} yielding the geodesics colored orange.

Note that aside from the tangent information, it is beneficial to exploit the original Eq. (4) to perform corrector steps that ensure one stays on the solution curve. These predictor-corrector methods [2,7] trace regular solution curves in general more efficiently than classical ODE solvers. However as our solution set fails to be a regular curve in the bifurcation point, one needs to be aware that after an inaccurate integration step followed by corrector steps one may end up on the wrong branch. To ensure the accuracy of the initial step we recommend using the second-order information (11).

Observe that we cannot obtain the second order information $\ddot{\varphi}_0$ in a focal cusp from the presented equations. However, the angle between the two branches there is actually $\frac{\pi}{2}$, making the initial integration step unproblematic. This is easily seen by comparing the tangents of the two branches and also visible in the numerical example depicted in Fig. 13 on the right.

Aside from the numerical examples presented in this papers, we have tested our approach not only with geodesics as homotopy curves but also in case Q is a regular non-geodesic curve tangentially meeting the focal curve. In all cases the method exhibited a numerically stable behavior. Thus, we consider it to be applicable as an efficient computational tool.

4 Applications

In this section we give a proof of concept for the geodesic bifurcation in order to outline its ability to capture distance related phenomena in various contexts. We strive for a presentation which illuminates the structure of ambiguity of connecting geodesics and how geodesic bifurcation is applied in this context. As an introductory example we illustrate how the HA profits in situations where geodesics present themselves as natural homotopy curves. Afterwards, considering examples, we discuss how to use geodesic bifurcation for computing distances on manifolds having a single closed focal curve.

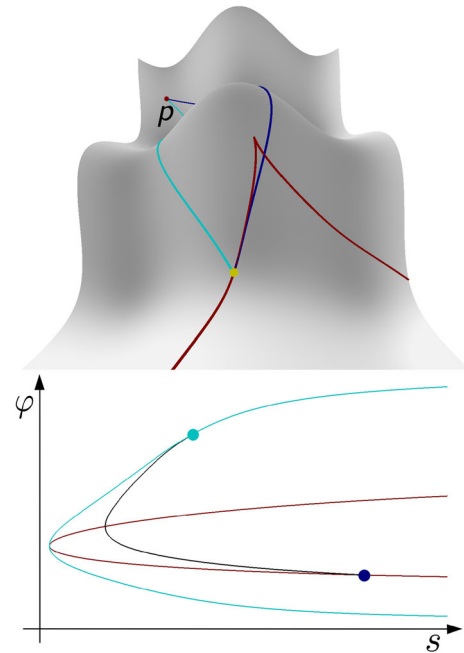


Fig. 14 Focal curve f_p and its preimage under O_p

We also discuss how to apply the geodesic bifurcation to solve the singularity of the medial differential equation in the focal cusp, providing starting points for tracing the locally induced cut locus branches. Furthermore we combine the medial equation and the HA in order to determine circumcircles as branching points of geodesic Voronoi diagrams. These considerations lead to a computational approach avoiding redundant tracing of medial segments by exploiting the examined natural starting points.

4.1 Introductory example

Figure 14 shows a generic situation on a height surface where a focal curve f_p is depicted in red. We consider the problem of determining the shortest paths from p to the focal curve f_p . This problem reduces to the computation of all connecting geodesics from p to points on f_p , i.e. to determining the preimage of f_p under O_p . We use the blue geodesic γ to apply geodesic bifurcation in the focal point q , colored yellow.

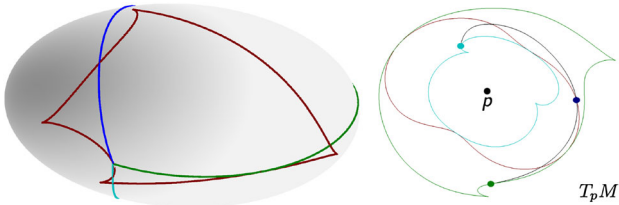


Fig. 15 Preimages of the focal curve under \exp_p

low. The solution branch of the geodesic bifurcation is shown in black in the parameter diagram. We follow this branch until reaching the cyan point, yielding the cyan geodesic.

In order to use the curve $f_p(\varphi)$ as a homotopy curve within the HA, observe that the coordinates of the cyan-colored point serve as suitable initial values. Thereby we obtain a family of geodesics tracing the focal curve, consisting of the shortest paths from p to f_p , represented by the cyan curve in the (s, φ) -plane.

In principle the classical HA could also yield the cyan geodesic. However, this would require the construction of a valid homotopy curve Q , i.e. one has to ensure that Q starts and ends outside of the region bounded by f_p , does not intersect f_p tangentially and passes through the endpoint of the blue geodesic. Furthermore one would have to provide suitable geodesic polar coordinates of some point on Q as initial values for tracing it. From an application point of view this is unsatisfying. However, note that in our context the blue geodesic is a priori given and thereby suggests itself to apply geodesic bifurcation.

Figure 15 shows an analogous situation on an ellipsoid. Applying geodesic bifurcation to the blue geodesic yields two other geodesics connecting p with the yellow focal point. Their GPCs serve as initial values for obtaining two families of geodesics tracing the focal curve. Again the cyan curve in the parameter diagram consists of the GPCs of the shortest paths from p to f_p .

4.2 Distance computation

Consider the ellipsoid shown in the sequence in Fig. 16, where the reference point p has been placed on its back side. The focal curve f_p of p is depicted in red and a point q (blue) is placed somewhere within the region bordered by f_p . Our goal is to determine the distance $d_M(p, q)$, which is accomplished by applying geodesic bifurcation.

First of all we easily obtain the black geodesic γ connecting p and q , shown in (a), using the HA as discussed in [34]. Now we extend γ until it generates the yellow focal point as indicated in (b). Applying geodesic bifurcation to γ yields a family of geodesics connecting p to points on γ . We distinguish between the geodesics tracing γ upwards colored in green respectively those tracing γ downwards,

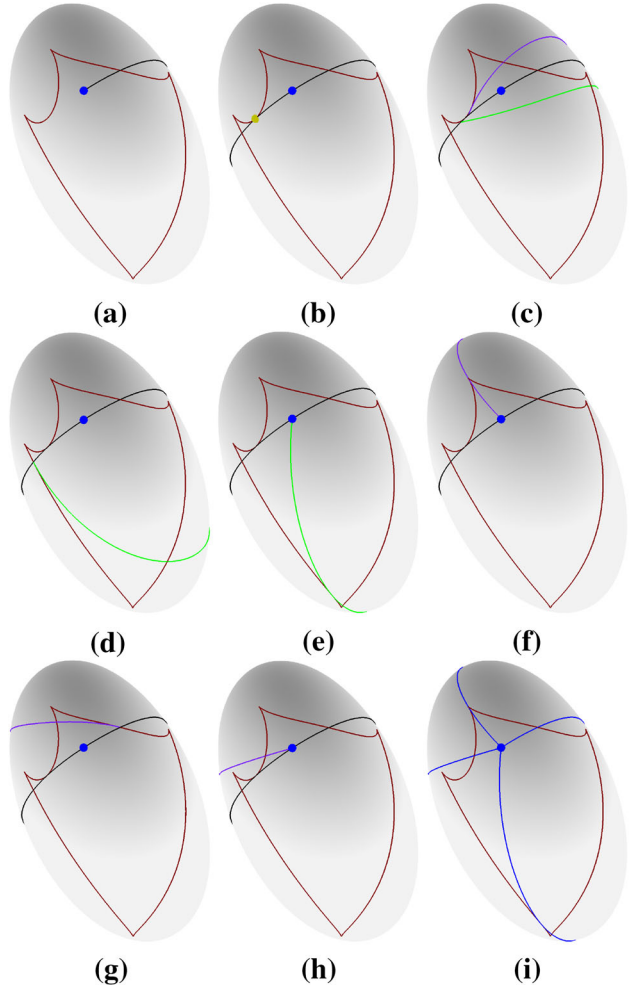
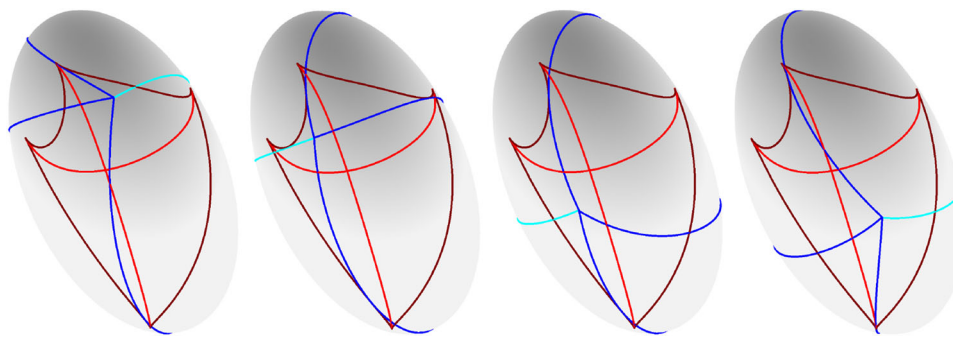


Fig. 16 Using geodesic bifurcation to compute distances on an ellipsoid

colored in purple, see (c). The green family reflects at f_p , cf. (d), where the depicted geodesic generates a focal point. The tracing continues downwards γ until we reach the configuration depicted in (e) where the green geodesic finally connects p and q . The family of purple geodesics analogously traces downwards γ yielding a first connecting geodesic as depicted in (f) before it reflects at f_p , see (g), and ends up in the configuration shown in (h) providing a fourth connecting geodesic. The geodesic bifurcation has yielded four connecting geodesics from p to q as shown in the final figure (i), including the shortest path from p to q .

Although we exemplified the idea of computing the distance on the ellipsoid in a particular example, the method described above applies to any configuration of p and q , where these points are separated by f_p . Thus the outlined approach always yields four (distance-) relevant connecting geodesics, meaning that one of them is guaranteed to be the (not necessarily unique) shortest path from p to q . This is illustrated in Fig. 17 where the symmetry set (light

Fig. 17 Distance relevant connecting geodesics



red) decomposes the region bordered by the focal curve into four sub-regions, see also [8]. The figure shows the resulting set of distance relevant geodesics for a point in each of those sub-regions, with the shortest path being marked in cyan. The blue geodesics all intersect the cut locus, being the longer vertical branch of the symmetry set.

Having discussed the most involved case, we can state, that the distance computation problem for all configurations of p and q is easily achieved by computing an initial connecting geodesic γ and applying geodesic bifurcation adequately.

Solving the distance problem using the presented approach is feasible in this case due to the fact that the considered ellipsoid has a single closed focal curve, implying that every geodesic generates a focal point and can therefore be used to apply geodesic bifurcation. We expect this method to generalize to similar surfaces with a closed focal curve as exemplified in Fig. 18, showing a distance-relevant set of connecting geodesics that has been obtained by applying geodesic bifurcation to the black geodesic.

4.3 Natural starting points

Having discussed elementary distance computations we turn our attention to finding natural starting points for a redundancy minimizing computation of cut loci. Please recall that the cut locus has a graph structure consisting of cut locus branches, which are subsets of corresponding medials characterized by the medial Eq. (3). In order to trace those medials we differentiate (3) with respect to λ and obtain the medial differential equation (MDE)

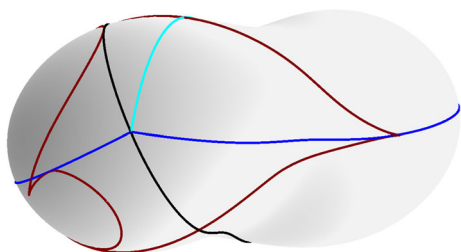


Fig. 18 Closed focal curve on a topological sphere

$$\frac{\partial O_p}{\partial s} \dot{s} + \frac{\partial O_q}{\partial \varphi} \dot{\varphi} = \frac{\partial O_q}{\partial s} \dot{s} + \frac{\partial O_q}{\partial \varphi} \dot{\psi}, \tag{12}$$

where the partial derivatives of O_p on the left are evaluated in (s, φ) , whereas on the right the corresponding parameters are given as (s, ψ) . Obviously a starting respectively end point on the medial is required to initiate respectively terminate the tracing process which can be performed using standard numerical methods, see e.g. [2,7].

Each cut locus branch has the topological structure of an interval which may be unbounded in one or both directions. If it terminates, the corresponding end point is either a focal cusp or circumcenter as described in Sect. 2. Therefore, in order to minimize redundant computations, we start the aforementioned tracing process in these terminal points if they exist and are known. If such points fail to exist as for example in some Voronoi diagram of two points p, q , we start tracing at the middle point of a distance minimizing geodesic connecting p with q . We will discuss each of those three natural starting points in the following three subsections.

4.3.1 Focal cusp

We will now consider cut locus branches which are locally induced. Here focal cusps serve as natural starting points for tracing these branches. However, as the MDE becomes singular in the focal cusp, an initial tangent of the symmetry set has to be obtained in a different manner. Recall Fig. 19 illustrating the behavior of the MDE near the focal cusp.

Considering Eq. (10) describing how to deal with the geodesic bifurcation there. It implies a symmetrical situation for the two appearing geodesics, as indicated by the green parabola shown in Fig. 13 on the right. This parabola is colored in black in the numerical example depicted in Fig. 19 on the right, approximating the light red preimage of the symmetry set under O_p .

Therefore taking a small Euler step using this tangent information in both directions yields two new geodesics (blue) providing suitable initial values for the MDE. After this step, one is able to continue a regular tracing process

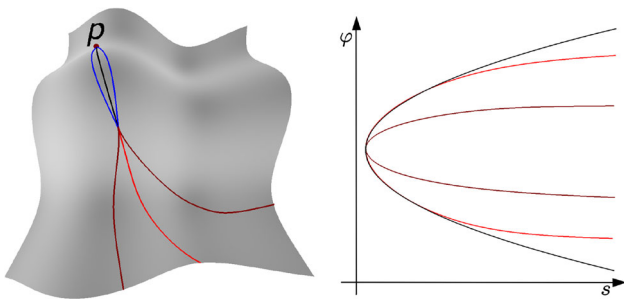


Fig. 19 Initial geodesics for the MDE and approximation (black) of the symmetry set (light red) in parameter space

as described by the MDE. Thus, the geodesic bifurcation gives access to the cut locus branch from its natural starting point in the focal cusp, as confirmed by the numerical example.

4.3.2 Middle point

As our second case we consider determining the cut locus $C_{\{p,q\}}$ of two points $p, q \in M$ for which no a-priori information about potential initial respectively terminal points is available. In order to obtain a natural starting point for this globally induced medial we determine a distance minimizing connecting geodesic and its mid point as illustrated in Fig. 20a (left). From this point we start the tracing process in both directions as shown in the other two pictures. Note that there appears to be a reflection behaviour of the considered medial that is examined briefly in the following.

Using the terminology of 3.1 we can phrase the tracing process in terms of two geodesic families tracing the medial branch. More precisely taking scalar products of equation (12) with $\frac{\partial O_p}{\partial s}$ respectively $\frac{\partial O_q}{\partial s}$ yields

$$\left(1 - \left\langle \frac{\partial O_p}{\partial s}, \frac{\partial O_q}{\partial s} \right\rangle\right) \dot{s} = \left\langle \frac{\partial O_q}{\partial \varphi}, \frac{\partial O_p}{\partial s} \right\rangle \dot{\psi}$$

$$\left(1 - \left\langle \frac{\partial O_q}{\partial s}, \frac{\partial O_p}{\partial s} \right\rangle\right) \dot{s} = \left\langle \frac{\partial O_q}{\partial \varphi}, \frac{\partial O_q}{\partial s} \right\rangle \dot{\psi}.$$

By subtraction we obtain

$$\left\langle \frac{\partial O_q}{\partial \varphi}, \frac{\partial O_q}{\partial s} \right\rangle \dot{\psi} = \left\langle \frac{\partial O_q}{\partial \varphi}, \frac{\partial O_p}{\partial s} \right\rangle \dot{\psi},$$

indicating $\dot{\psi}$ to vanish as soon as the tracing process of the medial branch passes a focal point with respect to p , where $\frac{\partial O_q}{\partial \varphi} = 0$. Vice versa we have that $\dot{\psi}$ vanishes if $\frac{\partial O_q}{\partial \varphi} = 0$. The vanishing of $\dot{\psi}$ indicates that the family of geodesics starting in p is reflected, which is immediate when incorporating the results of Sect. 3.1. Since the two families are coupled via Eq. (12) the endpoints of the family starting in q has to exhibit a similar behavior.

In our example the reflection of the family starting in p causes the medial to exhibit irregular points precisely at the focal curve f_p (dark red) as confirmed in Fig. 20b (left). The point of self-intersection is actually located on the cut locus C_p which is contained in $C_{\{p,q\}}$. After the considerations already discussed, the astute reader will realize that this implies the existence of another medial being locally induced with respect to p and terminating in the focal cusp of f_p , see Fig. 20b (middle). In order to obtain the Voronoi diagram $C_{\{p,q\}}$ these two medials have to be cut adequately as shown in Fig. 20b (right), emphasizing that several segments of the traced medials are in fact redundant.

Following up on the remark in 2.4 we note that the resulting geodesic Voronoi diagram exhibits a peculiar behaviour not usually observed due to the ordinary definition of Voronoi diagrams relying on Voronoi regions partitioning the underlying space with respect to the distance function. The generalized definition based on the cut locus encodes additional distance information as indicated by the lower branch shown

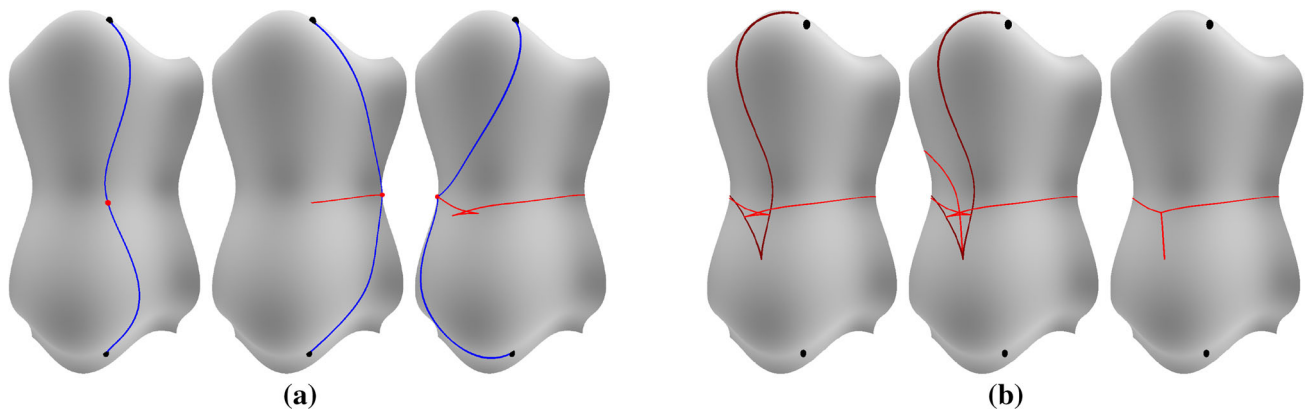


Fig. 20 Two-point Voronoi diagram in the presence of focal curves. **a** Tracing a medial with reflecting behaviour, starting from the midpoint of a connecting geodesic. **b** Symmetry set consisting of two medials, with the appropriate segments yielding the cut locus

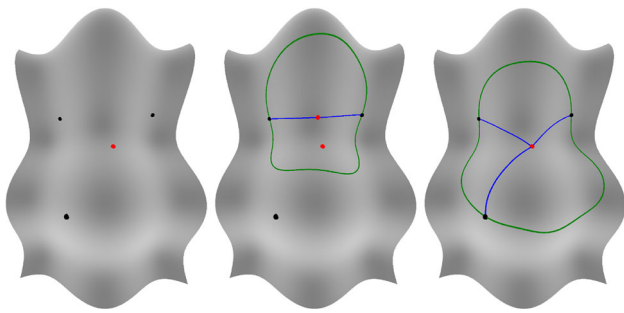


Fig. 21 Example for a circumcircle homotopy

in Fig. 20b (right) which is contained in the Voronoi region V_p associated with p . More precisely any geodesic connecting p with another point inside V_p is distance minimizing precisely when it does not intersect the mentioned branch.

It is now evident that incorporating the focal information with respect to p yields in fact two natural starting points, being the branching point b respectively the focal cusp c . The latter is locally accessible using the geodesic bifurcation as explained in Sect. 4.3.1 and should be preferred to start the complete cut locus tracing process, while it should terminate in c . The problem of detecting branching points during the tracing process leads us to the considerations in the next subsection.

4.3.3 Circumcenter

In order to detect a branching point we rely on the circumcircle characterization discussed in Sect. 2. As an example consider the three black sites illustrated in Fig. 21, where the point highlighted in red is the single branching point in their Voronoi diagram and therefore a natural starting point. We construct a family G_λ of geodesic circles with centers $m(\lambda) = O_{p_1}(s(\lambda), \varphi_1(\lambda))$ and radius $s(\lambda)$ which ends up in the desired circumcircle shown in the right picture by considering the equations

$$\begin{aligned} O_{p_1}(s(\lambda), \varphi_1(\lambda)) &= O_{p_2}(s(\lambda), \varphi_2(\lambda)) \\ O_{p_3}(s_3(\lambda), \varphi_3(\lambda)) &= O_{p_1}(s(\lambda), \varphi_1(\lambda)), \end{aligned} \tag{13}$$

where the first describes the medial between p_1 and p_2 , whereas the second specifies a geodesic connecting p_3 and the current point on the aforementioned medial. Differentiating this system with respect to λ one obtains a differential equation which combines the MDE and the HA to trace the family G_λ of circles, terminating in the desired circumcircle if $s_3(\lambda) \geq s(\lambda)$.

The tracing process starts with $\lambda = 0$ in the situation as depicted in Fig. 21 (middle). In order to obtain the corresponding initial parameters we determine the shortest connecting geodesic (blue) of p_1 and p_2 , the corresponding middle point $m(0)$ and additionally the shortest connecting geo-

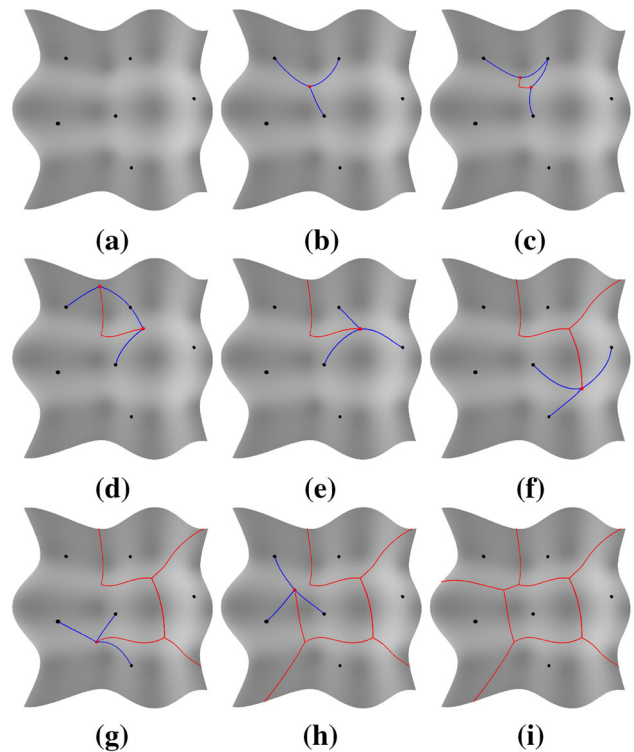


Fig. 22 Sequence of the tracing process of a geodesic Voronoi diagram with six sites

desic from p_3 to $m(0)$ (not shown) with $s_3(0) \geq s(0)$. We end up in the configuration illustrated in the right picture where the three involved geodesics (blue) are of equal length and thereby end up on the center $m(\lambda_1)$ of their circumcircle, which is the single branching point in their Voronoi diagram.

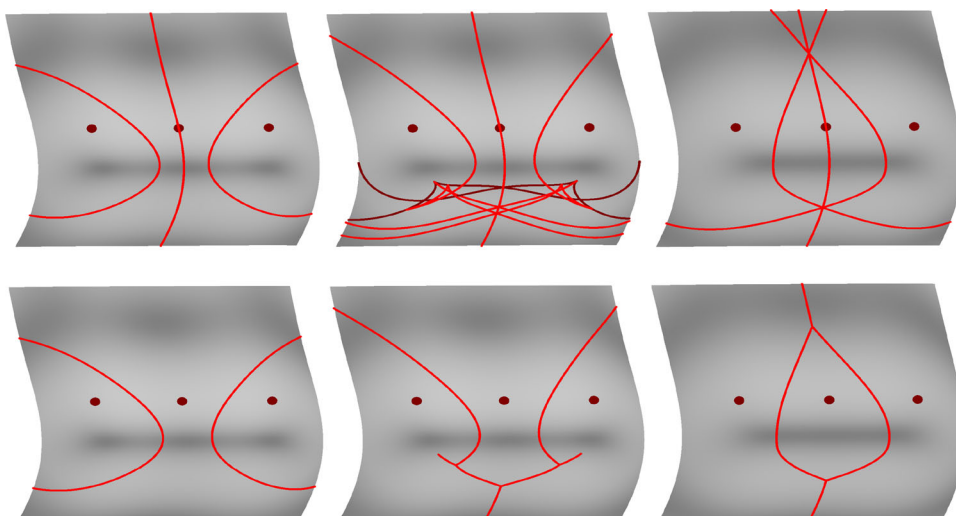
In the three site example obviously p_3 is the only site relevant to be considered for inducing a branching point of the Voronoi regions associated with p_1, p_2, p_3 . However in the presence of further sites p_4, \dots, p_n one easily extends the above method to detect when the medial of p_1 and p_2 enters the Voronoi region of any other site. For this purpose one merely has to append the additional equations

$$O_{p_k}(s_k(\lambda), \varphi_k(\lambda)) = O_{p_1}(s(\lambda), \varphi_1(\lambda)) \quad \text{for } k = 4, \dots, n.$$

to the system (13) and proceed analogously, stopping if $s(\lambda)$ becomes larger than any $s_k(\lambda)$ for $k = 3, \dots, n$.

We conclude by noting that although we used our methods mainly to discuss and understand the singularities of the exponential map in terms of the reflection behavior of the geodesic families involved, the circumcircle approach combining those methods with natural starting points as discussed in this paper avoids redundant tracing of medials. This is illustrated in our example depicting a geodesic Voronoi diagram of six sites on a curved surface with inherent focal curves of the reference sites shown in Fig. 22.

Fig. 23 Example for symmetry sets (upper row) and corresponding Voronoi diagrams computed on the manifold given by (14) with $\mu = 3.0, 2.9, 2.3$



4.4 Concluding example

Note that our methods are able to deal with highly non linear and curved manifolds with site constellations defining geodesic Voronoi diagrams whose topological structure depends inherently on the underlying Riemannian metric as indicated by our final example depicted in Fig. 23. Here a one parameter family of surfaces parametrized by

$$f(u, v) = (u, v, u^2 + v^2 + \mu(\cos(u) + \sin(v))) \quad (14)$$

with a perturbation parameter μ . To facilitate the visualization we have employed a stereographic projection diminishing the distracting distortions.

Comparing to our previous example in Fig. 20b (right) which might have raised the impression of being pathological in the sense that the observed additional branch might be a rare phenomenon, our final example shows that this behaviour generically occurs together with sudden topological changes as μ varies. More specifically for $\mu = 3.0$ the picture on the left topologically reminds of an Euclidean Voronoi diagram with three collinear sites. A small variation of μ produces a branching point and furthermore the appearance of two locally induced cut locus branches as shown in the middle. The corresponding symmetry set depicted above obviously contains several redundant medial segments which do not have to be traced when applying the discussed methods. A further variation of μ leads to the appearance of a closed Voronoi region with two branching points in the considered region. Remarkably, those two branching points are centers of two distinct circumcircles being described by the same three sites.

Note that our computational approach inspired by the smooth paradigm of classical Riemannian geometry allows to analyze and understand these commonly occurring multifarious phenomena.

5 Conclusion

In this follow-up on [34] we presented a solution to deal with the singularity occurring within the homotopy based approach proposed there. More precisely we have analyzed situations, where the homotopy curve meets the focal curve tangentially in a regular focal point and even in the focal cusp. A closer examination leads us to study the bifurcation of two transversally intersecting solution branches in parameter space. We have analytically investigated this bifurcation and exposed tangent and higher order information of these branches in terms of locally available information. Furthermore we have shown how to exploit this information for a numerically stable implementation within the homotopy approach.

Applications such as the medial axis or the cut locus, though being global concepts are related to the local concept of focal curves as classical theory predicts their branches to originate in the examined focal cusps. The computation of these concepts is efficiently and accurately performed tracing medial branches using the medial differential equation. Unfortunately the latter becomes singular in the origins of the medial branches. Having solved the geodesic bifurcation in the focal cusp we are able to provide two initial geodesics lying on the corresponding medial branch. Thereby using this result it is possible to naturally approach the medial branch from the focal cusp.

The geodesic bifurcation presented in this paper allows geodesics generating a focal point to be used as natural homotopy curves, dispensing the homotopy method in [34] from any restrictions. Furthermore in case of the commonly occurring locally induced non-injectivities of the exponential map, such a geodesic is always available and can be used to obtain a distance relevant set of connecting geodesics incorporating the HA adequately.

Especially for the illustrated surfaces with a single closed focal curve, where every geodesic generates a focal point, this is a valuable contribution. In this case, as we have discussed, the method is able to calculate the distance of arbitrary points. Contrary to previous approaches, this is done without requiring the explicit knowledge of the focal curve and without relying on the artificial construction of a homotopy curve. Thus, by incorporating the geodesic bifurcation presented in this paper, the homotopy approach unfolds its full potential in the context of distance calculation.

Furthermore we have shown how to apply the presented concepts for the computation of cut loci exploiting natural starting points using the geodesic bifurcation. By combining the HA and the medial differential equation we were able to capture the branching points of Voronoi diagrams. Thus, we were able to minimize redundant computations of segments of medials.

Although the geodesic bifurcation significantly improves upon the homotopy approach, it is limited since the general non-injectivities of the exponential map cannot completely be understood considering focal situations only. In general we can distinguish between two different origins for the appearance of multiple geodesic connections. One can be considered to be induced by Gaussian curvature in the presence of focal curves, whereas the other case is induced by the global topology of the surface. Having covered the local aspects of geodesic ambiguity, the global aspects of geodesic ambiguity remain theoretically and computationally challenging. The latter requires additional tools providing topologically distinct geodesic loops. This can be considered a large topic for future research.

While being beyond the scope of this work, please note that aside from the geodesic polar coordinates considered here our approach applies directly to the more general Fermi coordinates, too. In addition, due to the intrinsic setting only relying on the metric tensor, our methods apply to energy minimization as indicated by Maupertuis' principle. Furthermore, our method generalizes to pseudo-Riemannian spaces which can be investigated in an analogous way.

Acknowledgments This research was partially supported by a Deutsche Forschungsgemeinschaft (DFG) Grant within the Graduiertenkolleg 615.

References

- Abraham, R., Marsden, J.E., Ratiu, T.S., Cushman, R.: Foundations of mechanics. Benjamin/Cummings Publishing Company Reading, Massachusetts (1978)
- Allgower, E.L., Georg, K.: Numerical continuation methods. Springer (1990)
- do Carmo.: Riemannian Geometry. Birkhauser (1992)
- De Berg, M., Cheong, O., Van Kreveld, M., et al.: Computational geometry: algorithms and applications. Springer (2008)
- Dey, T.K., Li, K.: Cut locus and topology from surface point data. In: Proceedings of the 25th annual symposium on computational geometry, pp. 125–134 (2009)
- Dey, T.K., Zhao, W.: Approximating the medial axis from the voronoi diagram with a convergence guarantee. *Algorithmica* **38**(1), 179–200 (2003)
- Garcia, C., Zangwill, W.: Pathways to solutions, fixed points, and equilibria. Prentice, Englewood Cliffs (1981)
- Itoh, J.I., Kiyohara, K.: The cut loci and the conjugate loci on ellipsoids. *Manuscr. Math.* **114**(2), 247–264 (2004)
- Itoh, J.I., Sinclair, R.: Thaw: a tool for approximating cut loci on a triangulation of a surface. *Exp. Math.* **13**(3), 309–325 (2004)
- Kimmel, R., Sethian, J.: Computing geodesic paths on manifolds. *Proc. Natl. Acad. Sci.* **95**(15), 8431 (1998)
- Kunze, R., Wolter, F.-E., Rausch, T.: Geodesic voronoi diagrams on parametric surfaces. In: CGI, pp. 230–237 (1997)
- Landau, L., Lifshitz, E.: Mechanics. 3rd edn. Butterworth-Heinemann (2003)
- Leibon, G., Letscher, D.: Delaunay triangulations and voronoi diagrams for riemannian manifolds. In: Proceedings of the sixteenth annual symposium on computational geometry, pp. 341–349. ACM (2000)
- Liu, Y.J.: Exact geodesic metric in 2-manifold triangle meshes using edge-based data structures. *Computer-Aided Design* (2012).
- Liu, Y.J., Tang, K.: The complexity of geodesic voronoi diagrams on triangulated 2-manifold surfaces. *Inf. Process. Lett.* (2013)
- Misztal, M.K., Bærentzen, J.A., Anton, F., et al.: Cut locus construction using deformable simplicial complexes. In: Voronoi diagrams in science and engineering, pp. 134–141. IEEE (2011)
- Myers, S.B., et al.: Connections between differential geometry and topology. i. Simply connected surfaces. *Duke Math. J.* **1**(3), 376–391 (1935)
- Myers, S.B., et al.: Connections between differential geometry and topology ii. Closed surfaces. *Duke Math. J.* **2**(1), 95–102 (1936)
- Naß, H.: Computation of medial sets in Riemannian manifolds. Ph.D. thesis, LUH (2007)
- Naß, H., Wolter, F.-E., Dogan, C., et al.: Medial axis inverse transform in complete 3-dimensional Riemannian manifolds. In: cyberworlds, pp. 386–395 (2007)
- Naß, H., Wolter, F.-E., Thielhelm, H., et al.: Computation of geodesic Voronoi diagrams in 3-space using medial equations. In: cyberworlds, pp. 376–385 (2007)
- Neel, R., Stroock, D.: Analysis of the cut locus via the heat kernel. *Surv. Diff. Geom.* **9**, 337–349 (2004)
- Onishi, K., Itoh, J.I.: Estimation of the necessary number of points in riemannian voronoi diagram. In: Proceedings of 15th Canadian conference computer geometry, pp. 19–24 (2003)
- Patrikalakis, N.M., Maekawa, T.: Shape interrogation for computer aided design and manufacturing. Springer (2002)
- Polthier, K., Schmies, M.: Straightest geodesics on polyhedral surfaces. *ACM* (2006)
- Rausch, T.: Untersuchungen und Berechnungen zur Medialen Achse bei Berandeten Flächenstücken. Ph.D. thesis, Leibniz Universität Hannover (1999)
- Rausch, T., Wolter, F.-E., Sniehotta, O.: Computation of medial curves in surfaces. *Math. Surf.* **7**, 43–68 (1996)
- Sakai, T.: Riemannian geometry, vol. 149. American Mathematical Society (1996)
- Savage, L.: On the crossing of extremals at focal points. *Bull. Am. Math. Soc.* **49**(6), 467–469 (1943)
- Sinclair, R., Tanaka, M.: Loki: software for computing cut loci. *Exp. Math.* **11**(1), 1–25 (2002)
- Sinclair, R., Tanaka, M.: Jacobi's last geometric statement extends to a wider class of liouville surfaces. *Mathematics of computation* pp. 1779–1808 (2006)

32. Stam, J.: Exact evaluation of catmull-lark subdivision surfaces at arbitrary parameter values. In: computer graphics and interactive techniques, pp. 395–404 (1998)
33. Surazhsky, V., Surazhsky, T., Kirsanov, D., Gortler, S.J., Hoppe, H.: Fast exact and approximate geodesics on meshes. In: ACM TOG, vol. 24, pp. 553–560. ACM (2005)
34. Thielhelm, H., Vais, A., Brandes, D., et al.: Connecting geodesics on smooth surfaces. *The visual computer* pp. 1–11 (2012)
35. Wolter, F.-E.: Distance function and cut Loci on a complete Riemannian manifold. *Arch. Math.* **32**, 92–96 (1979)
36. Wolter, F.-E.: Cut Loci in bordered and unbordered Riemannian manifolds. Ph.D. thesis, TU Berlin (1985)
37. Wolter, F.-E.: Cut Locus and medial axis in global shape interrogation and representation. In: MIT design laboratory memorandum 92–2 (1992)
38. Wolter, F.-E., Blanke, P., Thielhelm, H., Vais, A.: Computational differential geometry contributions of thewelfenlab to grk 615. In: modelling, simulation and software concepts for scientific-technological problems, pp. 211–235, Springer (2011)
39. Wolter, F.-E., Friese, K.-I.: Local and global geometric methods for analysis interrogation, reconstruction, modification and design of shape. In: CGI, pp. 137–151 (2000)



Hannes Thielhelm obtained a diploma degree in Mathematics and Computer Science from the Leibniz University of Hannover in 2007. As a Ph.D. student he is currently involved with theoretical investigations and the design of algorithms for distance related problems in Riemannian geometry.



Alexander Vais gained a B.Sc. and M.Sc. degree in Computer Science from the Leibniz University of Hannover (LUH) in 2007 and 2009, respectively. He is currently a Ph.D. student at LUH Division of Computer Graphics. His main interests are computational differential geometry and geometry processing algorithms.



Franz-Erich Wolter has been Chaired Full Professor of Computer Science at Leibniz University Hannover since 1994 where he directs the Division of Computer Graphics called Welfenlab. He held faculty positions at University of Hamburg (1994), MIT (1989–1994) and Purdue University USA (1987–1989). He was software and development engineer with AEG (Germany) (1986–1987). Dr. Wolter obtained his Ph.D. (1985) mathematics, TU Berlin, Germany, in the area of Riemannian manifolds, Diploma (1980), FU Berlin, mathematics and theoretical physics. At MIT he co-developed the geometric modeling system Praxiteles for the US Navy and published papers that broke new ground applying concepts from differential geometry and topology on problems in geometric modeling. Dr. Wolter is research affiliate of MIT.